The University of
Nottingham

UNITED KINGDOM · CHINA · MALAYSIA

Fritz, Niklas and Rashed, Mohamed and Bozhko, Serhiy and Cuomo, Fabrizio and Wheeler, Pat (2018) Analytical modelling and power density optimisation of a single phase dual active bridge for aircraft application. In: 9th International Conference on Power Electronics, Machines and Drives (PEMD 2018), 17-19 April 2018, Liverpool, UK.

Access from the University of Nottingham repository:

http://eprints.nottingham.ac.uk/51425/1/Analytical%20modelling%20and%20power%20density%20optimisation%20of%20a%20single%20phase%20dual%20active%20bridge%20for%20aircraft%20application.pdf

Analytical Modeling and Power Density Optimization of a Single Phase Dual Active Bridge for Aircraft Application

Niklas Fritz[*], *Mohamed Rashed*[*], *Serhiy Bozhko*[*], *Fabrizio Cuomo*[†] *and Pat Wheeler*[*]

[*] *The Department of Electrical and Electronic Engineering, The University of Nottingham, United Kingdom*

[†] *Leonardo Aircraft Division, Naples, Italy*

niklas.fritz@rwth-aachen.de

Keywords: Dual Active Bridge, Modeling, Optimization, Power density, More Electric Aircraft

Abstract

A design procedure for the Dual Active Bridge (DAB) converter is presented, which aims to optimized power density and computational effort. When designing a DAB, the selection of circuit design parameters such as switching frequency, leakage inductance and semiconductor technologies is a complex question when targeting losses and weight minimization of the final design. In this paper, analytical models of the operating waveforms, the losses and the weight of all DAB components are developed. The proposed design algorithm is used for designing a 3 kW high frequency DAB for an aircraft DC power system.

1 Introduction

The concept of the More Electric Aircraft (MEA) promotes the use of electrical instead of traditional hydraulic, pneumatic or mechanical systems [1, 2]. The advantages are reduced cost, reduced fuel consumption, lower weight and less environmental impact. This results in an increase in the power rating of the aircraft power system and imposes the use of high voltage DC buses. Hence, DC/DC converters will play an important role in the management of electrical power in future aircraft. The ASPIRE project, part of the Clean Sky 2 Joint Undertaking, aims to design an electrical power system for next-generation aircraft. One goal of the ASPIRE project is to design an ultra-light and efficient Isolated Bidirectional DC/DC Converter (IBDC), interfacing the 28 V and 270 V DC buses at 3 kW rated power. The Dual Active Bridge (DAB) is a suitable topology [3] for such application.

The design of the DAB implies the choice of many converter parameters such as switching frequency, leakage and magnetizing inductances, semiconductor devices and transformer materials in order to minimize the total losses and weight of the converter. Such large numbers of design parameters make the design of the DAB a tedious and complex process.

Existing analytical modeling based design approaches rarely consider modeling of power losses or weight of converter components [4–8]. Moreover, many DAB designs are very specific to the target application [9–11].

In this paper, an efficient design procedure based on analytical modeling of the DAB is proposed and applied to optimize the converter for the highest power density with minimal computational effort. The proposed optimization technique, visualized in Fig. 1, consists of three steps. It starts with the calculation of the current and voltage waveforms and other electrical variables of the DAB, e.g. the RMS current. In the second step, those variables are used to assess converter losses. The third layer of the optimization technique is an analytical model of the component weights used to assess the power density.

The paper is organized in six sections, section 2 gives an overview of the DAB. Section 3 introduces the analytical model of the DAB operating waveforms. In sections 4 and 5, loss and weight analytical models are given. Finally, section 6 gives an example design of the DAB for the ASPIRE project.

2 The Single Phase Dual Active Bridge

The DAB was first proposed in 1991 [3] and its generic single phase variant is depicted in Fig. 2.

The single phase DAB consists of two active H-Bridges and a high frequency transformer. V_P and V_S denote the primary and secondary side DC voltages, respectively. The original modulation strategy is called Single Phase Shift Modulation (SPS), which is depicted in Fig. 3 [3]. Both H-Bridges operate at 50 % duty cycle, but phase shifted in time by the angle ϕ. The output voltages of the primary and secondary side H-Bridge are denoted $v_P(t)$ and $v_S(t)$, respectively. Using the transformer turns ratio n, all secondary side quantities are referred to the primary side and indicated by a dash. The waveforms $v_P(t)$ and $v'_S(t)$ are shown in Fig. 3a. The voltage difference $v_P(t) - v'_S(t)$ drops across the leakage inductance L of the transformer and results in a quasi-square wave AC current in the transformer,
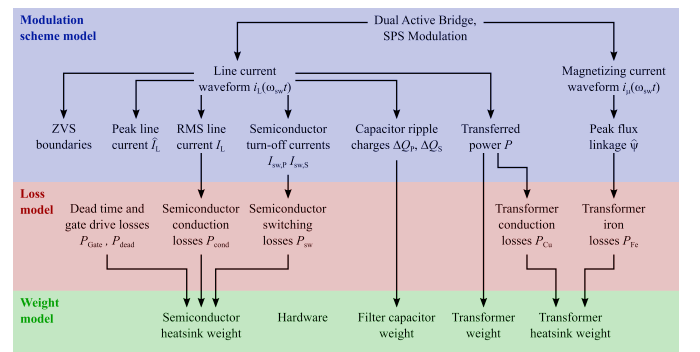

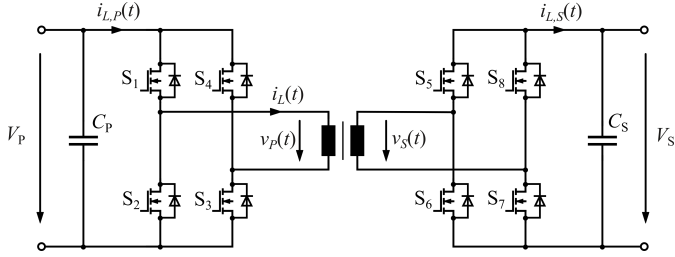Figure 1: Flowchart of the proposed design algorithm.

1

Figure 2: The Dual Active Bridge topology, single phase.

$i_L(t)$ (see Fig. 3c). As shown in Fig. 2, the input currents of the primary and secondary side H-Bridge are denoted $i_{L,P}(t)$ and $i'_{L,S}(t)$, respectively. They are plotted in Fig. 3d and Fig. 3e, respectively. The current ripples are filtered by the DC-link capacitors C_P and C_S. The average currents provided by the primary and secondary side DC buses are denoted $\bar{I}_{L,P}$ and $\bar{I}'_{L,S}$. The transferred power P is given in (1), where ϕ denotes the phase shift angle between $v_P(t)$ and $v'_S(t)$ and f_{sw} denotes the switching frequency [3].

$$P = \frac{V_P V'_S}{2\pi^2 f_{sw} L} \cdot \phi \left(\pi - |\phi|\right) \tag{1}$$

Maximum power is transferred for a phase shift angle of $\pi/2$ and the turn-off of the devices in both H-Bridges is generally hard-switched, but for the turn-on, zero voltage switching (ZVS) is achieved for most operating points.

3 Analytical Model of SPS Modulation

Before analyzing the losses and the weight of the DAB, the analytical model of SPS modulation is derived from two current waveforms, namely the current $i_L(\omega_{sw}t)$ in the AC link and the magnetizing current $i_\mu(\omega_{sw}t)$. Because of waveform symmetries (see Fig. 3), it is sufficient to regard half a switching period. The following conventions are made, which are visualized in Fig. 4: For positive phase shifts $\phi \geq 0$, the rising edge of the primary voltage $v_P(t)$ is located at $\omega_{sw}t = 0$ and the rising edge of the secondary voltage $v'_S(t)$ is delayed to $\omega_{sw}t = \phi$. For negative phase shifts $\phi < 0$, the rising edge of the secondary voltage is located at $\omega_{sw}t = 0$ and the rising edge of the primary voltage is delayed to $\omega_{sw}t = |\phi|$.

3.1 Line Current and Derived Quantities

The current waveform $i_L(\omega_{sw}t)$ is obtained by integrating the output voltage difference of the H-Bridges, $v_P(t) - v'_S(t)$. For keeping the model simple, ohmic resistances and the magnetizing inductance L_m are neglected. The resulting current waveform as well as its initial values at $\omega_{sw}t = 0$ and $\omega_{sw}t = |\phi|$ are given as follows:

$$i_L(\omega_{sw}t) = \begin{cases} i_L(0) + \mathrm{sgn}(\phi) \frac{V_P + V'_S}{\omega_{sw}L} \omega_{sw}t \\ \qquad \text{for } 0 \leq \omega_{sw}t < |\phi| \\ i_L(|\phi|) + \frac{V_P - V'_S}{\omega_{sw}L} (\omega_{sw}t - |\phi|) \\ \qquad \text{for } |\phi| \leq \omega_{sw}t < \pi \end{cases} \tag{2}$$
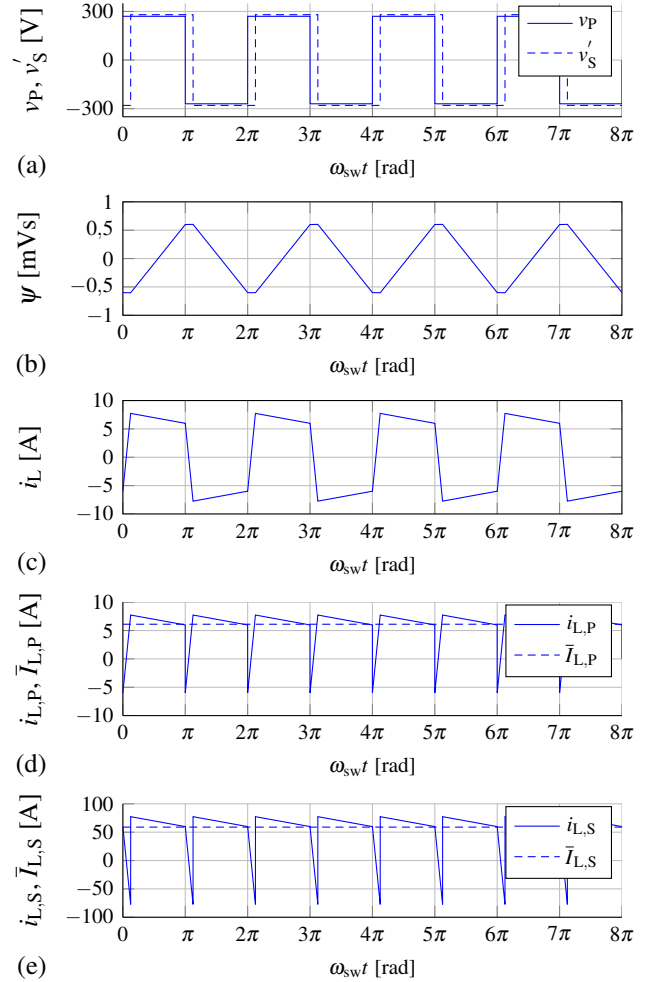

(a)

(b)

(c)

(d)

(e)

Figure 3: The generic Single Phase Shift (SPS) modulation. (a) Output voltages of the H-Bridges. (b) Transformer flux linkage. (c) AC link current. (d) Primary side rectified current and primary side DC current. (e) Secondary side rectified current and secondary side DC current.

$$i_L(0) = -\frac{1}{2} \left(\frac{V_P + V'_S}{\omega_{sw}L} \phi + \frac{V_P - V'_S}{\omega_{sw}L} (\pi - |\phi|) \right) \tag{3}$$

$$i_L(|\phi|) = +\frac{1}{2} \left(\frac{V_P + V'_S}{\omega_{sw}L} \phi - \frac{V_P - V'_S}{\omega_{sw}L} (\pi - |\phi|) \right) \tag{4}$$

Depending on the sign of the phase shift angle ϕ, the two H-Bridges either switch at the time instant $\omega_{sw}t = 0$ or $\omega_{sw}t = |\phi|$. For example, for $\phi \geq 0$, the primary H-Bridge switches at $\omega_{sw}t = 0$ and for $\phi < 0$, it switches at $\omega_{sw}t = |\phi|$. Therefore, it is important to calculate the current which has to be switched off by the H-Bridges, regardless of the respective time instant. For the primary and the secondary H-Bridges, the turn-off currents are given in (5) and (6), respectively.

$$I_{sw,P} = -\frac{1}{2} \left(\frac{V_P + V'_S}{\omega_{sw}L} |\phi| + \frac{V_P - V'_S}{\omega_{sw}L} (\pi - |\phi|) \right) \tag{5}$$

$$I'_{sw,S} = +\frac{1}{2} \left(\frac{V_P + V'_S}{\omega_{sw}L} |\phi| - \frac{V_P - V'_S}{\omega_{sw}L} (\pi - |\phi|) \right) \tag{6}$$

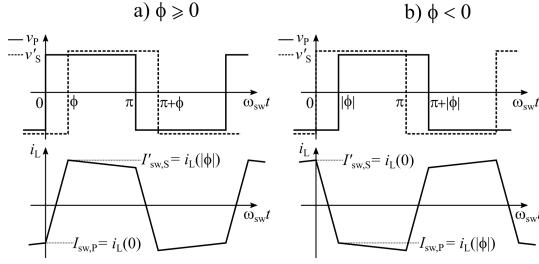From (5) and (6), the conditions for ZVS of the primary and

2

Figure 4: Timing conventions for the analytical models.

secondary side H-Bridge, respectively, are derived. At the turn-off instant, the current flows in the antiparallel diode of the switches. This is formulated as follows:

$$I_{\text{sw,P}} < 0 \implies V_{\text{P}} > V_{\text{S}}' \left(1 - 2\frac{|\phi|}{\pi}\right) \tag{7}$$

$$I_{\text{sw,S}}' > 0 \implies V_{\text{S}}' > V_{\text{P}} \left(1 - 2\frac{|\phi|}{\pi}\right) \tag{8}$$

As $|\phi| \leq \pi/2$, the second term in (7) and (8) is always positive. It is clear that if the ratio of the DC voltages does not match the transformer turns ratio n, i.e. $V_{\text{P}} \neq V_{\text{S}}'$, the ZVS conditions will be violated at low load [12].

The peak value of the AC link current i_{L} is denoted $\hat{I}_{\text{L}}$:

$$\begin{aligned}
\hat{I}_{\text{L}} &= \max\left[|i_{\text{L}}(0)|,\ |i_{\text{L}}(|\phi|)|\right] \\
&= \frac{|V_{\text{P}} - V_{\text{S}}'|}{2\omega_{\text{sw}}L}\pi + \frac{(V_{\text{P}} + V_{\text{S}}') - |V_{\text{P}} - V_{\text{S}}'|}{2\omega_{\text{sw}}L}|\phi|
\end{aligned} \tag{9}$$

By squaring (2) and integrating, the RMS value of the AC link current, I_{L}, is also derived:

$$I_{\text{L}} = \frac{1}{\omega_{\text{sw}}L}\sqrt{\frac{\pi^2}{12}(V_{\text{P}} - V_{\text{S}}')^2 + V_{\text{P}}V_{\text{S}}'\left(\phi^2 - \frac{8}{12\pi}|\phi|^3\right)} \tag{10}$$

The input currents of the two H-Bridges, $i_{\text{L,P}}(t)$ and $i_{\text{L,S}}'(t)$, as shown in Fig. 3d and Fig. 3e, are obtained by changing the sign of i_{L} in a way such that it accounts for the switching state of the respective H-Bridges. From the waveforms, the average DC currents $\bar{I}_{\text{L,P}}$ and $\bar{I}_{\text{L,S}}'$ are obtained by averaging:

$$\bar{I}_{\text{L,P}} = \frac{V_{\text{S}}'}{\pi\omega_{\text{sw}}L}\phi(\pi - |\phi|) \tag{11}$$

$$\bar{I}_{\text{L,S}}' = \frac{V_{\text{P}}}{\pi\omega_{\text{sw}}L}\phi(\pi - |\phi|) \tag{12}$$

Multiplying the currents (11) and (12) with the respective DC voltage yields the power transfer equation (1). If pure DC currents are assumed at the two ports of the DAB, the current ripples of $i_{\text{L,P}}(t)$ and $i_{\text{L,S}}'(t)$ are assumed to flow into the DC-link capacitors C_{P} and C_{S}. The ripple charges ΔQ_{P} and $\Delta Q_{\text{S}}'$ are derived from the areas enclosed by the waveforms $\left(i_{\text{L,P}}(\omega_{\text{sw}}t) - \bar{I}_{\text{L,P}}\right)$ and $\left(i_{\text{L,S}}'(\omega_{\text{sw}}t) - \bar{I}_{\text{L,S}}'\right)$. The results are shown in equations (29) and (30).

The required DC-link capacitor sizes are calculated by dividing the ripple charges given in (29) and (30) by the permissible voltage ripples ΔV_{P} and ΔV_{S}. The energies needed to be stored in the capacitors C_{P} and C_{S} are given by E_{CP} and E_{CS} in (13) and (14), respectively.

$$E_{\text{CP}} = \frac{1}{2}C_{\text{P}}(V_{\text{P}} + \Delta V_{\text{P}})^2 = \frac{V_{\text{P}}^2\Delta Q_{\text{P}}}{2\Delta V_{\text{P}}} + V_{\text{P}}\Delta Q_{\text{P}} + \frac{\Delta V_{\text{P}}\Delta Q_{\text{P}}}{2} \tag{13}$$

$$E_{\text{CS}} = \frac{1}{2}C_{\text{S}}(V_{\text{S}} + \Delta V_{\text{S}})^2 = n\left(\frac{V_{\text{S}}^2\Delta Q_{\text{S}}'}{2\Delta V_{\text{S}}} + V_{\text{S}}\Delta Q_{\text{S}}' + \frac{\Delta V_{\text{S}}\Delta Q_{\text{S}}'}{2}\right) \tag{14}$$

3.2 Magnetizing Current and Derived Quantities

The transformer is modeled by its T-equivalent circuit, which is shown in Fig. 5. The inductances $L_{\text{P}\sigma}$ and $L_{\text{S}\sigma}'$ describe the leakage inductances of the transformer on both the primary and secondary windings, so that $L = L_{\text{P}\sigma} + L_{\text{S}\sigma}'$. The ratio of leakage inductances r, the ratio of voltages d and the transformer utilization factor λ are defined as follows (15)-(17):

$$r = \frac{L_{\text{P}\sigma}}{L_{\text{S}\sigma}'} \tag{15}$$

$$d = \frac{V_{\text{P}}}{V_{\text{S}}'} \tag{16}$$

$$\lambda = 1 - \frac{|V_{\text{P}} - rV_{\text{S}}'|}{V_{\text{P}} + rV_{\text{S}}'} = 1 - \frac{|d - r|}{d + r} \tag{17}$$

Using definitions (15)-(17) and the assumption that the leakage inductances are much smaller than L_{m}, the virtual voltage v_{m} on the magnetizing inductance can be calculated from the circuit in Fig. 5 as in (18):

$$v_{\text{m}}(t) = \frac{v_{\text{P}}(t) + rv_{\text{S}}'(t)}{1 + r} = \begin{cases} v_{\text{P}}(t) & \text{for } r = 0 \\ \frac{v_{\text{P}}(t) + v_{\text{S}}'(t)}{2} & \text{for } r = 1 \\ v_{\text{S}}'(t) & \text{for } r \to \infty \end{cases} \tag{18}$$

By integrating the voltage of equation (18), the magnetizing current waveform $i_\mu(\omega_{\text{sw}}t)$ is obtained:

$$i_\mu(\omega_{\text{sw}}t) = \begin{cases} i_\mu(0) + \text{sgn}(\phi)\frac{V_{\text{P}} - rV_{\text{S}}'}{(1+r)\omega_{\text{sw}}L_{\text{m}}}\omega_{\text{sw}}t \\ \qquad \text{for } 0 \leq \omega_{\text{sw}}t < |\phi| \\ i_\mu(|\phi|) + \frac{V_{\text{P}} + rV_{\text{S}}'}{(1+r)\omega_{\text{sw}}L_{\text{m}}}(\omega_{\text{sw}}t - |\phi|) \\ \qquad \text{for } |\phi| \leq \omega_{\text{sw}}t < \pi \end{cases} \tag{19}$$

$$i_\mu(0) = -\frac{1}{2}\left(\frac{V_{\text{P}} - rV_{\text{S}}'}{(1+r)\omega_{\text{sw}}L_{\text{m}}}\phi + \frac{V_{\text{P}} + rV_{\text{S}}'}{(1+r)\omega_{\text{sw}}L_{\text{m}}}(\pi - |\phi|)\right) \tag{20}$$

$$i_\mu(|\phi|) = +\frac{1}{2}\left(\frac{V_{\text{P}} - rV_{\text{S}}'}{(1+r)\omega_{\text{sw}}L_{\text{m}}}\phi - \frac{V_{\text{P}} + rV_{\text{S}}'}{(1+r)\omega_{\text{sw}}L_{\text{m}}}(\pi - |\phi|)\right) \tag{21}$$

The flux linkage in the transformer core is given by $\psi = L_{\text{m}}i_\mu$ (see Fig. 3b). In analogy to (9), the peak magnetizing current $\hat{I}_\mu$
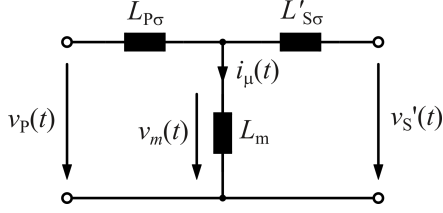
3

Figure 5: T-equivalent circuit of the transformer.

and the peak flux linkage $\hat{\psi}$ are calculated:

$$
\begin{aligned}
\hat{I}_\mu &= \max\left[|i_\mu(0)|,\ |i_\mu(|\phi|)|\right] \\
&= \frac{V_P + rV_S'}{2(1+r)\omega_{sw}L_m}\pi - \frac{(V_P + rV_S') - |V_P - rV_S'|}{2(1+r)\omega_{sw}L_m}|\phi| \quad (22)
\end{aligned}
$$

$$
\hat{\psi} = \frac{V_P + rV_S'}{2(1+r)\omega_{sw}}\pi - \frac{(V_P + rV_S') - |V_P - rV_S'|}{2(1+r)\omega_{sw}}|\phi| \quad (23)
$$

From (23), it becomes clear that the maximum peak flux linkage in the transformer core, $\hat{\psi}_{max}$, is given as follows:

$$
\hat{\psi}_{max} = \frac{V_P + rV_S'}{2(1+r)\omega_{sw}}\pi \quad (24)
$$

The flux density B cannot be calculated as the number of turns and the core area are still unknown. However, if a reasonable value is assumed for the maximum flux density $\hat{B}_{max}$, the per-unit utilization of the transformer can be derived as given by (25), based on the utilization factor λ defined in (17).

$$
\frac{\hat{B}}{\hat{B}_{max}} = \frac{\hat{\psi}}{\hat{\psi}_{max}} = 1 - \lambda\frac{|\phi|}{\pi} \quad (25)
$$

4 Analytical Loss Model

A loss model is required to evaluate efficiency and the cooling effort. For the DAB under design, MOSFETs are used. The conduction losses are calculated using the on-state resistances $R_{DS,P}$ and $R_{DS,S}$ of the MOSFETs in the primary and secondary side H-Bridges, respectively. The AC link current always flows through two switches of each H-Bridge simultaneously. Also the transformer contributes to conduction losses with its total equivalent copper resistance R_{Cu}. High-frequency loss components due to skin and proximity effects are neglected for simplicity. Therefore, the total conduction losses of the converter, $P_{cond,tot}$, are expressed as a function of a total equivalent resistance R_{tot}:

$$
R_{tot} = 2R_{DS,P} + 2n^2 R_{DS,S} + R_{Cu} \quad (26)
$$
$$
P_{cond,tot} = R_{tot}\cdot I_L^2 \quad (27)
$$

The share of conduction losses with respect to the transferred power, $P_{cond,tot}/P$, is plotted as a function of the phase shift angle in Fig. 6. The maximum phase shift should be limited to a value below the theoretical limit of $\pi/2$, to enhance efficiency.
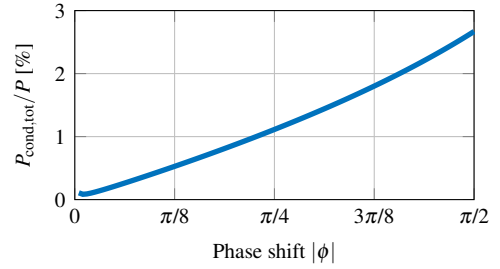

Figure 6: Share of conduction losses in transferred power. $V_P = 270\,\mathrm{V}$, $V_S = 28\,\mathrm{V}$, $n = 10$, $f_{sw} = 100\,\mathrm{kHz}$, $L = 25\,\mu\mathrm{H}$, $R_{tot} = 0.2\,\Omega$.

Furthermore, the overall power which is required to drive the power MOSFETs is calculated using their gate charges $Q_{g,P}$ and $Q_{g,S}$ and the gate voltages $V_{g,P}$ and $V_{g,S}$:

$$
P_{gate} = 4f_{sw}Q_{g,P}V_{g,P} + 4f_{sw}Q_{g,S}V_{g,S} \quad (28)
$$

During the dead time periods $t_{d,P}$ and $t_{d,S}$, the body diodes of the power MOSFETs conduct, causing additional losses due to

$$
\Delta Q_P = \begin{cases}
\dfrac{(2V_S'\phi^2 + \pi^2(V_P - V_S'))^2}{8\omega_{sw}^2 L\pi^2(V_P - V_S')} & \text{for } V_P > V_S' \text{ and } |I_{sw,S}'| < |\bar{I}_{L,P}| \\[2ex]
\dfrac{(2V_S'|\phi|(2\pi - |\phi|) + \pi^2(V_P - V_S'))^2}{8\omega_{sw}^2 L\pi^2(V_P + V_S')} & \text{for } \begin{cases} V_P = V_S' \text{ or} \\ V_P > V_S' \text{ and } |I_{sw,S}'| \geq |\bar{I}_{L,P}| \text{ or} \\ V_P < V_S' \text{ and } |I_{sw,P}| \geq |\bar{I}_{L,P}| \end{cases} \\[3ex]
\dfrac{V_S'(2V_S'\phi^2 - (\pi^2 - 2\pi|\phi|)(V_P - V_S'))^2}{4\omega_{sw}^2 L\pi^2(V_S'^2 - V_P^2)} & \text{for } V_P < V_S' \text{ and } |I_{sw,P}| < |\bar{I}_{L,P}|
\end{cases} \quad (29)
$$

$$
\Delta Q_S' = \begin{cases}
\dfrac{V_P(2V_P\phi^2 + (\pi^2 - 2\pi|\phi|)(V_P - V_S'))^2}{4\omega_{sw}^2 L\pi^2(V_P^2 - V_S'^2)} & \text{for } V_P > V_S' \text{ and } |I_{sw,S}'| < |\bar{I}_{L,S}'| \\[2ex]
\dfrac{(2V_P|\phi|(2\pi - |\phi|) - \pi^2(V_P - V_S'))^2}{8\omega_{sw}^2 L\pi^2(V_P + V_S')} & \text{for } \begin{cases} V_P = V_S' \text{ or} \\ V_P > V_S' \text{ and } |I_{sw,S}'| \geq |\bar{I}_{L,S}'| \text{ or} \\ V_P < V_S' \text{ and } |I_{sw,P}| \geq |\bar{I}_{L,S}'| \end{cases} \\[3ex]
\dfrac{(2V_P\phi^2 - \pi^2(V_P - V_S'))^2}{8\omega_{sw}^2 L\pi^2(V_S' - V_P)} & \text{for } V_P < V_S' \text{ and } |I_{sw,P}| < |\bar{I}_{L,S}'|
\end{cases} \quad (30)
$$

4

the forward voltage drop $V_{SD,P}$ and $V_{SD,S}$:

$$P_d = 4f_{sw} \cdot \left(t_{d,P} V_{SD,P} |I_{sw,P}| + t_{d,S} V_{SD,S} |nI'_{sw,S}| \right) \quad (31)$$

The switching losses of the MOSFETs are hard to describe analytically and as the DAB operates under ZVS, only the turn-off losses have to be considered. For estimating the switching losses, it is possible to use the following approaches, which are sorted in decreasing order of accuracy and in increasing order of ease of implementation:

1. Experimental data
2. Device models by the manufacturers
3. Switching loss data from the datasheets
4. Analytical estimates, e.g. as shown in [13]

Finally, the iron losses of the transformer are calculated using the improved generalized STEINMETZ equation (iGSE):

$$P_{Fe} = Vol_{Fe} f_{sw} \int_0^{f_{sw}^{-1}} k_i \left| \frac{dB}{dt} \right|^{\alpha} \Delta \hat{B}_{pp}^{\beta-\alpha} dt, \text{ where} \quad (32)$$

$$k_i = \frac{k}{(2\pi)^{\alpha-1} \int_0^{2\pi} |\cos\theta|^{\alpha} \cdot 2^{\beta-\alpha} d\theta} \quad (33)$$

k, α and β are material specific data, Vol_{Fe} is the iron volume and $\Delta \hat{B}_{pp}$ is the peak-to-peak core flux density. The cross-sectional area of the core and the number of turns are unknown design information. Therefore, the per-unit quantity $\mathcal{B}/\hat{b}_{max}$ from (25) is used in (32), which now can be solved analytically:

$$P_{Fe} = 2^{\alpha+\beta} Vol_{Fe} k_i f_{sw}^{\alpha} \hat{B}_{max}^{\beta} \left(1 - \lambda \frac{|\phi|}{\pi}\right)^{\beta-\alpha} \left(1 - \lambda_{\alpha} \frac{|\phi|}{\pi}\right) \quad (34)$$

$$\text{where } \lambda_{\alpha} = 1 - \left(\frac{|d-r|}{d+r}\right)^{\alpha}$$

The transformer core volume can be calculated using the stored energy E_m. It is expressed by the peak flux linkage and the magnetizing current on the one hand and by the peak flux density on the other hand:

$$E_m = \frac{1}{2} L_m \hat{I}_{\mu}^2 = \frac{1}{2} \hat{\psi}_{max} \hat{I}_{\mu} = Vol_{Fe} \cdot \frac{\hat{B}_{max}^2}{2\mu_0 \mu_r}$$

$$\Rightarrow Vol_{Fe} = \frac{\mu_0 \mu_r \hat{\psi}_{max} \hat{I}_{\mu}}{\hat{B}_{max}^2} \quad (35)$$

5 Analytical Weight Model

In this section, all components of the DAB as well as the losses are mapped to weights. Losses affect the weight in terms of the size of the heat sink. Its thermal resistance is denoted $R_{th,HS}$. Research [14] proposes a figure of merit, which is a material constant, to estimate the weight of a heat sink m_{HS}.

$$FOM_{HS} = \frac{1}{m_{HS} \cdot R_{th,HS}} \quad (36)$$

The weight of the input and output capacitors is proportional to the stored energy. To evaluate the weight, energy densities of suitable capacitor technologies may be researched.

Literature [15] states that the weight of the transformer m_{Tr} is proportional to the area product A_p, i.e. the product of core area A_c and winding window area A_w, by a factor K_W:

$$m_{Tr} = K_W \cdot A_p^{3/4} \quad (37)$$

Describing the window area in terms of the copper fill factor k_u, the number of turns N, the peak current density $\hat{J}_{max}$ and the maximum AC link RMS current $I_{L,max}$, and describing the core area in terms of maximum flux linkage $\hat{\psi}_{max}$ and maximum flux density $\hat{B}_{max}$, the area product is found:

$$A_p = A_c \cdot A_w = \frac{\hat{\psi}_{max}}{N\hat{B}_{max}} \cdot \frac{2NI_{L,max}}{k_u \hat{J}_{max}} = \frac{2P_{max}}{4f_{sw}k_u \hat{B}_{max} \hat{J}_{max}} \quad (38)$$

An alternative to this approach is to research existing transformers and find empirical relationships of weight and power.

6 Optimization Example

Combining the equations from the previous sections connects basic design parameters to the weights of the DAB components and enables optimization of power density. As an example, a preliminary design of the DAB of the ASPIRE project is presented in this section. Table 1 lists the converter parameters. The analysis is performed for a wide range of switching frequencies and different MOSFETs, including modern SiC and GaN devices. For minimization of the conduction losses, the maximum phase shift is reduced below the theoretical limit of $\pi/2$. This decides the leakage inductance according to (1).

Table 1: Parameters of the ASPIRE converter design.

DC voltages	V_P, V_S	270 V, 28 V
Rated power	P	3 kW
Ambient temperature	T_{amb}	70 °C
Switching frequency	f_{sw}	50 … 1000 kHz
Transformer turns ratio	n	10
Max. SPS phase shift angle	$|\phi|_{max}$	45°
Max. magnetizing current	$\hat{I}_{\mu}$	1 A
Max. junction temperature	$T_{j,max}$	125 °C
Max. transformer temperature	$T_{Tr,max}$	125 °C
Permissible ripple voltages	ΔV_P, ΔV_S	4 V, 1 V
Magnetic material	Ferroxcube	3C96
Maximum flux density	B_{max}	$0.5 \cdot B_{sat}$
Primary side MOSFETs	Infineon	IPT65R033G7 (Si)
	Wolfspeed	C3M0065090J (SiC)
	GaN Systems	GS66516T (GaN)
Secondary side MOSFETs	Infineon	IPT012N08N5 (Si)
	EPC	4x EPC2021 (GaN)

For estimating the switching losses, the equations from [13] are used. The thermal figure of merit for an aluminum cooling system including fan is needed. From the results of [16, 17], a value of $FOM_{HS} = 15 \frac{W}{kg\,K}$ is a reasonable choice. Additionally, for the filter capacitors C_P and C_S, a research of ceramic capacitors with suitable voltage ratings gave power densities of $41 \frac{J}{kg}$ and $19 \frac{J}{kg}$, respectively. For the transformer, an efficiency of 99 % is assumed, yielding a copper resistance of $R_{Cu} = 0.2\,\Omega$. A ratio of $r = 1$ for the leakage inductances is assumed. Planar

transformers with similar power ratings from different companies have been researched and the following empirical weight model has been fitted to the collected data:

$$m_{\text{Tr}} \approx 1.59 \, \frac{\text{kg}}{\sqrt{\text{W/Hz}}} \cdot \sqrt{\frac{P}{f_{\text{sw}}}} \qquad (39)$$
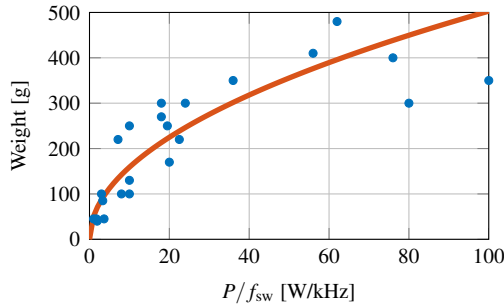
Figure 7: Weight data of existing planar transformers and empirical model.

The researched transformers weights as well as the empirical model from (39) are shown in Fig. 7. The STEINMETZ material parameters k, α and β are obtained from the loss density graphs from the datasheet. Moreover, a net weight of 140 g for the PCB, the hardware, the semiconductors and additional circuitry as gate drivers and sensors is assumed.

In Fig. 8, the theoretical power density for this example design is shown. The proposed target design is indicated by the dot. It reaches a power density of $6 \, \frac{\text{kW}}{\text{kg}}$ at $f_{\text{sw}} = 250 \, \text{kHz}$. Finally, Fig. 9 shows the weight and the loss breakdown of the design which is indicated by the dot in Fig. 8. Generating those results in MATLAB requires few seconds of computation time.
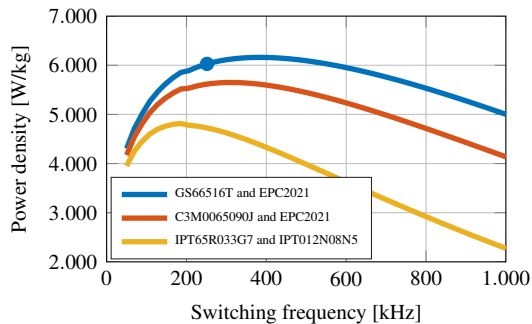
Figure 8: Power density as a function of switching frequency.

7 Conclusion

In this paper, analytical models of the operating waveforms, the losses and the component weights of a single phase DAB are developed and used in a design optimization algorithm. The design approach is easy to implement and is computationally efficient. The developed design optimization algorithm is a useful tool for the designer to obtain initial and fast designs of DAB and to identify the impact of specific design decisions on the power density of the DAB.
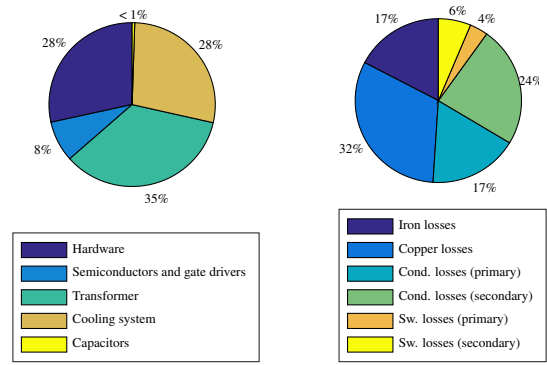
Figure 9: Left: Weight breakdown of the example design (total weight: 500 g). Right: Loss breakdown at $P = 3 \, \text{kW}$ of the example design (total losses: 111 W).

Acknowledgment

References

[1] P. Wheeler and S. Bozhko. 'The More Electric Aircraft: Technology and challenges'. In: *IEEE Electrification Magazine* 2.4 (2014), pp. 6–12.

[2] P. Wheeler. 'Technology for the more and all electric aircraft of the future'. In: *2016 IEEE International Conference on Automatica (ICA-ACCA)*. 2016.

[3] R. W. De Doncker et al. 'A Three-phase Soft-Switched High-Power-Density dc /dc Converter for High-Power Applications'. In: *IEEE Transactions on Industry Applications* 27.1 (1991), pp. 63–73.

[4] C. Fontana et al. 'Design characteristics of SAB and DAB converters'. In: *Intl. Conference on Optimization of Electrical & Electronic Equipment (OPTIM)*. IEEE, 2015.

[5] H. van Hoek et al. 'Performance analysis of an analytical calculation tool for dual-active-bridge converters'. In: *IEEE International Conference on Power Electronics and Drive Systems*. IEEE, 2015.

[6] A. Rodriguez et al. 'Different Purpose Design Strategies and Techniques to Improve the Performance of a Dual Active Bridge With Phase-Shift Control'. In: *IEEE Transactions on Power Electronics* 30.2 (2015), pp. 790–804.

[7] H. Choi et al. 'Design methodology of dual active bridge converter for solid state transformer application in smart grid'. In: *International Conference on Power Electronics and ECCE Asia (ICPE-ECCE Asia)*. IEEE, 2015.

[8] B. Zhao et al. 'A Synthetic Discrete Design Methodology of High-Frequency Isolated Bidirectional DC/DC Converter for Grid-Connected Battery Energy Storage System Using Advanced Components'. In: *IEEE Transactions on Industrial Electronics* 61.10 (2014), pp. 5402–5410.

[9] F. Krismer and J. W. Kolar. 'Efficiency-Optimized High-Current Dual Active Bridge Converter for Automotive Applications'. In: *IEEE Transactions on Industrial Electronics* 59.7 (2012), pp. 2745–2760.

[10] C. Gammeter et al. 'Comprehensive Conceptualization, Design, and Experimental Verification of a Weight-Optimized All-SiC 2 kV/700 V DAB for an Airborne Wind Turbine'. In: *IEEE Journal of Emerging and Selected Topics in Power Electronics* 4.2 (2016), pp. 638–656.

[11] P. Joebges et al. 'Design method and efficiency analysis of a DAB converter for PV integration in DC grids'. In: *IEEE Southern Power Electronics Conference (SPEC)*. IEEE, Dec. 2016.

[12] S. Taraborrelli et al. 'Bidirectional dual active bridge converter using a tap changer for extended voltage ranges'. In: *2016 18th European Conference on Power Electronics and Applications (EPE '16 ECCE Europe)*. Institute of Electrical and Electronics Engineers (IEEE), Sept. 2016.

[13] Vishay Intertechnology, Inc. *Device Application Note AN608A - Power MOSFET Basics: Understanding Gate Charge and Using it to Assess Switching Performance*. 2016. URL: http://www.vishay.com/doc?73217.

[14] T. Icoz and M. Arik. 'Light Weight High Performance Thermal Management With Advanced Heat Sinks and Extended Surfaces'. In: *IEEE Transactions on Components and Packaging Technologies* 33.1 (Mar. 2010), pp. 161–166.

[15] W. T. McLyman. *Transformer and Inductor Design Handbook*. New York: Marcel Dekker, Inc., 2004.

[16] C. Gammeter et al. 'Weight Optimization of a Cooling System Composed of Fan and Extruded-Fin Heat Sink'. In: *IEEE Transactions on Industry Applications* 51.1 (2015), pp. 509–520.

[17] P. Ning et al. 'Selection of heatsink and fan for high-temperature power modules under weight constraint'. In: *Twenty-Third Annual IEEE Applied Power Electronics Conference and Exposition*. 2008.